Polar stratospheric clouds over Antarctica from the CALIPSO spaceborne lidar

Vincent Noel, Albert Hertzog, Hélène Chepfer, David M. Winker

Polar Stratospheric Clouds over Antarctica from the CALIPSO Spaceborne Lidar

Vincent Noel[1], Albert Hertzog[2], Hélène Chepfer[2], David M. Winker[3]

[1] Laboratoire de Météorologie Dynamique / Institut Pierre-Simon Laplace, CNRS

[2] Laboratoire de Météorologie Dynamique / Institut Pierre-Simon Laplace, Université Pierre et Marie Curie

[3] NASA Langley Research Center

Submitted in *Journal of Geophysical Research* on March 6th 2007.

Revised version submitted on July 2nd 2007.

Second revised version submitted on October 2nd 2007.

Corresponding author : Vincent Noel, LMD, Ecole Polytechnique, 91128 Palaiseau, France. vincent.noel@lmd.polytechnique.fr

Abstract

This paper presents statistics of Polar Stratospheric Clouds (PSCs) above Antarctica from June to October 2006 using observations from the CALIOP spaceborne lidar, part of the CALIPSO mission. Synoptic-scale changes in their geographic and temporal distribution are documented on a weekly basis and correlated with temperature fields. A very high spatial and temporal variability tends to contradict the hypothesis that PSCs are mostly created via slow processes mainly governed by large-scale temperature changes. Linear depolarization ratios reveal strongly typed PSCs with distinct characteristics (implying different microphysics), but most of the time a unique cloud composition cannot be singled out. A West/East imbalance is observed in the depolarization distribution, symptomatic of microphysical disparities. A classification based on depolarization and scattering ratios suggests more than 60% of mixed PSCs, followed by more than 20% of STS, and a roughly equal concentration of NAT-based and pure ice PSCs (~8%). Up to the beginning of August, STS PSCs experience a steady decrease in concentration correlated with an increase in ice-based PSCs ; this tendency gets reversed after the first week of August.

1. Introduction

PSCs are traditionally classified according to their composition, either (Type Ia) a crystalline solid mixture of ice water with HNO_3-based particles such as nitric acid trihydrate (NAT) or dihydrate (NAD); (Type Ib) a liquid supercooled ternary solution of HNO_3, H_2SO_4 and H_2O; or (Type II) pure water ice (WMO, 2003). Inside Type Ia PSCs, a large number of small NAT crystals is designated as “enhanced NAT” (Tsias et al. 1999), while the presence of large particles in small numbers is termed “NAT-rock” (Fueglistaler et al. 2002); each play an important role in stratospheric denitrification. The composition itself depends on several factors, including the concentration of atmospheric chemical components, of nucleation particles, and the sufficiently long exposition of these components to temperatures low enough for clouds to form. Depending on these factors, a large number of interacting mechanisms are now considered to explain PSC formation (Höpfner et al. 2006), ranging from slow nucleation processes, mainly governed by synoptic-scale temperature changes (Teitelbaum et al., 2001) to rapid crystal formation due to mountain waves (e.g. Eckermann et al. 2006). On the surface of crystals, chemical reactions transform passive reservoir compounds (e.g. HCl) into active chlorine and bromine species that cause rapid ozone loss in sunlit conditions through destructive catalytic cycles (Solomon, 1999). Moreover, sedimenting crystals from Type I and II PSCs scavenge nitric acid with them (Jensen et al. 2002), slowing down further the conversion of active chlorine back to passive reservoir species. Due to these combined effects, PSCs are of fundamental importance to the formation of the Antarctic ozone hole (Farman et al. 1985). As the ongoing global climate change leads to stratospheric cooling (Randel, 2001), potentially increasing the population of PSCs and their impact on the ozone layer, it is of primary importance to better understand the spatial distribution and formation mechanisms producing these clouds.

Difficult living conditions in Antarctica make local observations sparse. Ground-based studies (David et al. 1998; Santacesaria et al. 2001; Blum et al. 2005) or in-situ measurements (Browell et al. 1990; Toon et al. 1990) give useful insights into the local properties of PSCs, but cannot account for their spatial variability across immense Antarctica. Existing PSC climatologies are either based on passive remote sensing observations (Poole et al. 1989, Poole and Pitts 1994) with a poor sensitivity to optically thin clouds (Hervig et al. 2001), or based on local ground-based stations (Adriani et al. 2004) with limited spatial

cover. Occultation techniques and limb observations (Spang et al. 2001; Fromm et al. 2003; Spang et al., 2005) give encouraging insights into PSC climatologies, but their spatial and temporal resolutions are limited and large differences exist between results from different instruments (Pavolonis and Key, 2003). The present paper aims to overcome these limitations by using backscatter and linear depolarization ratio δ (depolarization ratio hereafter) from the CALIOP (*Cloud-Aerosol Lidar with Orthogonal Polarization*) spaceborne lidar, an instrument well suited to PSC observations thanks to its vertical and horizontal resolutions and its high sensitivity to optically thin clouds.

The Geosciences Laser Altimeter System (Spinhirne et al. 2005a) was the first spaceborne lidar to look at PSCs (Palm et al. 2005a) ; the analysis of two days of observation suggested a correlation between PSCs and tropospheric disturbances (Palm et al. 2005b). Recent results from GLAS show a cloud cover 40% higher than from passive remote sensing (Spinhirne et al. 2005b), confirming the lidar suitability to thin cloud study ; however, GLAS lack the microphysical information contained in the depolarization ratio δ (Sassen, 1991) and was only operated during limited time periods that were not optimal for the observation of PSC variability – within the 12 available observation periods, the most appropriate one (September 25-November 18, 2003, used in Palm et al. 2005b) is already past the end of the peak PSC season. To provide the spatiotemporal variability needed for PSC studies requires a more extensive dataset, such as the one from CALIOP.

This paper presents a study of PSC properties over Antarctica during the 2006 austral winter, documenting the variability of their geographical and thickness distribution. A comprehensive dataset of spaceborne lidar observations (Sect. 2) provides 1) a high resolution and sensitivity especially suited to PSC detection, and 2) an extensive observation domain and period which allow to track synoptic-scale changes on a weekly scale during the season (Sect. 3.1 and 3.2). Depolarization ratio shows changes in the microphysical properties of PSCs (Sect. 3.3). Results are discussed in Sect. 4.

2. Observations and cloud detection

CALIOP is part of the NASA / CNES (*Centre National d'Etudes Spatiales*) mission CALIPSO (*Cloud Aerosol Lidar and Infrared Pathfinder Satellite Observations*), and orbits Earth roughly 14 times a day between 82°N and 82°S at 705 km (Winker et al. 2003, 2006). CALIOP has shown excellent agreement with airborne lidars during validation cam-

paigns (McGill et al. 2007) ; preliminary studies suggest its depolarization ratio follows distributions and trends inferred from long-term, ground-based studies (e.g. Sassen and Benson, 2001). These studies give confidence that CALIOP data is not affected by any significant bias and that scientific interpretation is possible. CALIOP time series are gathered on a non-uniform altitude and time grid (Winker et al. 2004) ; data was therefore first regridded over constant altitude bins of 30 meters, then averaged over 30 profiles, reducing the resolution from 1 profile every 333 meters (CALIOP's nominal resolution) to 1 profile every 10 km to improve signal-to-noise ratio.

The present study uses two and a half months of observation, from June 16 to August 31st – the period of maximum PSC occurrence above Antarctica – with 6 missing days (July 11 to 13 and 28, August 29 and 30). Data include total attenuated backscatter for 532 and 1064 nm channels (giving the color ratio), and attenuated backscatter in the 532 nm perpendicular channel (giving δ, Sect. 3.3) as a function of altitude, longitude and latitude (Hostetler et al. 2006). Due to solar light, daytime observations suffer from a relatively low signal-to-noise ratio which makes the detection of optically thin clouds not trivial and impacts the depolarization ratio ; however, given CALIPSO's heliosynchronous orbit, all clouds in the studied period and area – from 82°S to 65°S – were observed during nighttime. Observations with a signal-to-noise ratio below 3 in the 532 nm channel were discarded. Since more than 99% of PSCs during that period were optically thin (optical depth below 0.3) and frequently subvisual (optical depth below 0.03), multiple scattering effects should be negligible (You et al. 2006).

The cloud detection algorithm used in this study first normalizes individual profiles of total attenuated backscatter on the molecular backscattering profile in the middle stratosphere (between 28 km and 30 km, above possible PSC layers). Atmospheric features are detected on a profile-by-profile basis using a thresholding on the scattering ratio (i.e. a ratio between atmospheric and molecular backscatter higher than 1.15, following Massoli et al. 2006). In a given lidar profile referenced by time, latitude and longitude, a 30-m altitude bin with a scattering ratio higher than this threshold was identified as a "cloud point". PSC statistics (Sect. 3) were then obtained by analyzing the relevant data at cloud coordinates (time, latitude, longitude, altitude). Since there are no dependable statistics of color ratio (defined as the ratio between total backscattered intensity at 1064 and 532 nm) in PSCs, this measurement was used as an indicator of non-physical data – negative or saturated

values were filtered out. Fig. 1 shows an example of PSC observed by CALIOP on July 24, 2006 (average profile in the right panel) and the results of the cloud detection (Fig. 1b), with clear-sky in white. The number of false positives is low and does not affect the results; however extremely weak backscatter PSCs (e.g. profiles 1375 to 1450, at 13-15 km altitude) can be missed. Given how depolarization was averaged (Sect. 3.3) such clouds would have limited to no impact, but PSC thickness and cover (Sect. 3.1) could be underestimated. Further work will be required to verify the importance and extent of PSCs with scattering ratios below 1.15.

3. PSCs above Antarctica

During southern hemisphere winter, the lapse-rate definition of tropopause is not appropriate above Antarctica (Hudson and Brandt, 2005), hence a conservative value of 13 km was chosen as the lower altitude limit for the stratosphere. Cloud points above that altitude were considered as PSCs, and only data above this level was used in the study.

3. 1. Cloud Occurrence and Thickness

A lidar profile was considered as cloudy if at least 3 consecutive cloudy points (which translates to a cloud layer 100 m thick) were detected between 13 and 28 km. From this result, cloud occurrence in a lat-lon cell was defined as the number of cloudy lidar profiles divided by the entire number of profiles available in a given cell. Considering 7-day periods from June 16 to August 31, cloud occurrence in 2.5° x 2.5° cells poleward of 65°S (Fig. 2, column 1) is often greater than 50% (i.e. at least one profile out of two contains at least three cloud points). Over the continent it is consistently higher than 50% (saturated areas in Fig. 2 col. 1), and often reaches 100% (i.e. all profiles in a cell contain at least three cloud points). Until July 8th, clouds are mostly located in the East hemisphere; from then on clouds are present in both hemispheres until August. After August 8, maximum occurrences drop below 50% and are only widespread south of 75°S. In the last two weeks of August, cloud occurrences drop to very low values close to the pole; occurrences are still important (>30%) further away from the pole (north of 75°S), but these are thin clouds (Fig. 2, col. 2).

The number of cloud points per profile higher than 13 km can be translated into cloud thickness, and averages from 0 (clear sky) to 150 (4.5 km cloud thickness) in a given cell.

Geometrically thicker clouds are generally closer to South Pole, at or south of 76°S (Fig. 2, col. 2). Thick clouds are geographically heterogeneous, their location is variable from one week to the next, and is rather well correlated with cloud occurrence and temperature. PSCs are rather thin during the beginning of winter, apart from regional areas of high cloud occurrence over the peninsula in the Eastern hemisphere (June 24 to July 7). Cloud thickness then increases rapidly, with thick clouds covering more or less the entire Antarctic continent between July 24 and 31 and covering a quarter of diagram (30°W to 120°W, north of 62°S) between August 1st and 7. During that week, the associated backscatter is higher than July 1-15 observations by an order of magnitude. During the following week (August 8-15) clouds more than 1 km thick still appear over large portions of Antarctica (especially 75°W-120°W and 0°-60°E), but their overall surface is greatly reduced. Between August 16 and 31, PSCs almost never get thicker than 1 km, and those thicker than 500 m are located far away from the Pole (North of 75°S, consistent with cloud occurrence).

3. 2. Temperature

PSC particle types are traditionally associated with a maximum threshold temperature depending on their supposed formation process - 195 K for Type Ia (NAT) and Ib (STS), 188 K for Type II (ice), at the 60 hPa level (roughly in mid-stratosphere) and 3 ppmv water mixing ratio (Savigny et al. 2005). The transition from a sulfuric- to nitric-acid dominated solution in Type Ib PSC occurs in a small temperature window (~2 K), 3 to 5 K warmer than the ice frostpoint (Lowe et al. 2006). Given that the altitude (13-28 km) and pressure (20-120 hPa) ranges considered here are large, these temperature thresholds are subject to some variations.

Fig. 1c shows the geographic distribution of the minimum temperature at the 530K isentropic surface (21 km in average), using the same grid as in Sect. 3.1. ECMWF temperatures have a maximum uncertainty of +3.5/-2.5 K in the Austral polar vortex (Gobiet et al. 2005). If homogeneous freezing were the main mechanism of PSC formation, cloud cover would be homogeneous in areas colder than 185 K (blue in Fig. 2, col. 3). Comparing temperatures with cloud occurrence (Fig. 2, col. 1) and thickness (Fig. 2, col. 2) shows that being colder than the homogeneous nucleation threshold is not enough to form PSCs. However, highest cloud concentrations clearly occur at coldest temperatures (July 24-

August 7), which suggests that homogeneous freezing can occur relatively fast on a weekly scale when temperatures are well below the condensation point (Drdla and Browell, 2004). The correlation with temperature is not as good after August 8th. More work is needed to conclude on the dominant formation processes based on temperatures in PSCs (Sect. 4).

Temperature distribution in cloud points (Fig. 3) indicates that PSCs are present between 175 K and 200 K, with most of them appearing within 180 - 190 K (consistent with results from Savigny et al. 2005). The distribution peaks at 182 - 184 K, with a sharp drop towards colder temperatures. It appears monomodal, but analysis of data subsets in distinct regions and time periods suggests it is a combination of overlapping modes. These modes are most likely linked to distinct PSC types, but attempts to separate modes based on other measurements (e.g. depolarization) did not bring any significant result.

3. 3. Depolarization Ratio Observations

Lidar observations in the 1990's (Browell et al. 1990, Toon et al. 1990) showed PSCs can depolarize (solid, Type Ia, II) or not (liquid, Type Ib). It is generally agreed that microphysical properties of PSCs can be inferred from parallel and perpendicular lidar signal (e.g. Biele et al. 2001), however ground-based lidar observations from Dumont d'Urville have shown that the temperature-depolarization relationship is complex (Stefanutti et al. 1995), with non-depolarizing PSCs below the NAT freezing threshold and vice-versa.

Depolarization ratio maps (Fig. 2, col. 4) were obtained by 1) separately totalling signal in the perpendicular and parallel planes in stratospheric cloud points (Sect. 2) in all profiles observed inside individual grid cells over 7 days, and 2) computing the ratio of both (Sassen et al. 2001). Parallel-plane signal was obtained by substracting perpendicular backscatter channel signal from the total backscatter channel signal. This averaging technique minimizes the influence of small-scale fluctuations due to noise, but, all things being equal, implies that PSCs with stronger backscatter will dominate the average values. It should be noted that other statistics, such as distributions, were obtained by considering separate values of depolarization ratio at individual cloud coordinates (time,lat,lon,altitude). Among those, the number of physically unrealistic depolarization ratios (i.e. greater than 0.8) stays below 2%.

The average δ in cloud points (Fig. 2, col. 4) varies significantly from one week to the next. Areas of high cloud concentration do not produce a stable δ, which ranges generally between 0.3 and 0.5 and suggests heterogeneous microphysical properties.

- The area of highest cloud concentration and thickness (45°W to 120°W, August 1st to 7) shows high average δ, slightly above 0.4. Similar values are also observed the previous week (July 24 to 31), scattered in the Western part of the diagram. These clouds are extremely widespread (synoptic-scale) and correlated with the arrival of extremely low temperatures (Sect. 3.2).

- High δ is also observed close to the Antarctic peninsula (i.e. 65°W) at rather low latitudes (north of 75°S) between June 24 and July 15. A detailed histogram of individual values of δ over this area and period shows a bimodal distribution: one mode close to 0.4 (extending up to 0.6) and another weak mode centered on 0. These clouds only cover a limited area (Fig. 2 col. 1), so they are not a statistically significant part of the PSC population. However, since they appear so brightly on the δ diagrams they must dominate the perpendicular signal - i.e. their backscattering is significantly higher than other clouds in that area, which typically suggests higher optical depths. Individual orbits reveal that the associated clouds reach mid-stratosphere (higher than 26 km), and indeed produce strong backscattering. These clouds are most likely orographic, associated with large-amplitude gravity waves (Hertzog et al. 2002; Dörnbrack et al. 2002) induced by the steep slopes of the Antarctic peninsula and the Ellsworth mountain. Locations and dates are consistent with observations from Höpfner et al. 2006.

- Apart from these two regions, average δ are most frequently close to 0.3. The depolarization ratio distribution over most areas shows a single mode – this suggests that these areas are either dominated by (1) a single type of PSC microphysics; or (2) a mixture of different particle types which produce the same depolarization ratio. In both cases, it is not possible without additional observations to describe the involved particle types with certainty.

- A last category of clouds (mostly in the first 3 weeks, for instance July 1-7 between 60 and 120°E) shows a very low δ, with a distribution centered on zero. This low-δ PSC category shows up in cloud occurrence (Fig. 2 col. 1) but is rather thin (Fig. 2 col. 2) and produces low backscattering. However, it represents a significant part of the overall cloud population, as a zero-depolarization mode appears in the global distribution.

Clouds colder than 188 K, located between 16 and 24 km (Fig. 4), produce relatively high δ, up to 0.6 with most observations between 0 and 0.4. Depolarization is strongly dependent on the vertical thermal profile, but is lower here than in clouds observed in the Arctic region by Massoli et al. (2006). By contrast, clouds warmer than 188 K are either located low in the stratosphere (13-16 km) or very high (above 24 km) and produce comparatively low δ, the majority below 0.25. δ appears geographically asymmetrical, as statistics over the entire period shows that $\delta > 0.2$ are mostly located in the Western area, while PSCs in the East mostly produce $\delta < 0.2$. High values in the West are not limited to the Peninsula, but generally happen above the continent. This asymmetry mirrors the one observed in tropopause cirrus in 2003 by Spinhirne et al. (2005a) using GLAS observations, and suggests a relationship between stratospheric and tropospheric processes as in Palm et al. (2005b). It can be due to orographic conditions (the Antarctic peninsula but also its Western coastline feature large elevation changes), but can also be linked to temperature variations.

Type Ib PSCs produce a low $\delta < 0.04$ (Browell et al. 1998; Toon et al. 2000); this is observed in ~18% of the present individual CALIOP cloud points. Mapping the concentrations of Type Ib PSCs shows a very homogeneous geographic distribution, without the strong local variations found in cloud thickness maps (Fig. 2 col. 1). Results were refined using the classification scheme from Massoli et al. (2006), which allow a separate identification of NAT, NAT rock, NAT enhanced, STS and ice PSCs, while staying consistent with classifications from Browell et al. (1998), Stein et al. (1999) and Dörnbrack et al. (2002). This scheme classifies PSCs according to observations of depolarization ratio and scattering ratios (Table 1 in Massoli et al. 2006). Following Massoli and Adriani et al. (2004), the scattering ratio SR was replaced by the (1-1/SR) parameter, in order to constrain the value in the (0,1) range. Fig. 5 shows the distribution of PSCs according to this scheme using a logarithmic color scale. The percentage of PSC types as a function of time (Fig. 6) shows a

strong dominance by mixed PSCs (62% in average), followed by STS PSCs (21%) and roughly equal quantities of NAT-based (8.2%) and ice PSCs (7.8%). NAT-based PSC concentrations are stable (7-10%); all other types experience stronger variations. The most variable are STS and Ice PSCs, and their evolution is anticorrelated : STS PSCs concentration goes down from 40% in mid-june to 15% in the first week of August, while Ice PSC concentration goes from 2% to 18% ; this evolution is inverted during the remaining of August (STS concentration goes back up to 30% while Ice PSCs go back to almost 0%). NAT Rock and enhanced NATs dominate NAT-based PSCs, with a very small fraction of pure NAT clouds. This last result should be treated with caution however, as NAT Rock PSCs cannot be identified unambiguously as by Fahey at al. (2001).

4. Discussion and Conclusions

This article describes the evolution PSC cover over Antarctica during two and a half months of the 2006 Austral winter, using spaceborne lidar observations which provide a resolution and sensitivity unreachable through passive remote sensing. Large variations in the geographical distribution of PSCs are documented from one week to the next, and the important role played by temperature in PSC formation is confirmed. Almost all PSCs were below the NAT freezing point (195 K), with a large fraction below the Type II PSC formation threshold (188 K) and a maximum cloud presence at even colder temperatures (~183 K). There is a high correlation between temperature and PSC occurrence and thickness, but temperature thresholds alone are not sufficient to explain the cloud geographic distribution, as its complexity shows compared to the temperature field and the polar vortex. Cloud distribution is most likely also strongly dependent on the distribution of pressure, water vapour and particle nuclei in the stratosphere. Temperature can therefore provide strong hints at the areas susceptible to contain PSCs and their subsequent type, but by itself is not sufficient to predict both. To conclude on the dominant PSC formation processes (heterogeneous or homogeneous), would require 1) the modelling of nucleation temperature threshold for the different particle types found in PSCs based on thermodynamical parameters, and 2) the colocated extraction of these parameters from other instruments within the A-Train (such as MLS). These steps are however out of the scope of the present paper and outline the basis of a future study.

Above the Antarctic circle the number of unphysical depolarization ratios stays low, so results should be considered robust ; this number however increases steadily from less than

0.5% at 82°S to almost 2% closer to 60°S, this effect might be due to the increase in solar light at the edges of the arctic circle and winter period, further studies should investigate. There is a strong relationship between temperature and depolarization ratio, with highly depolarizing clouds generally colder than 188 K (16-24 km) and non-depolarizing PSCs warmer than 188 K. This dependence, also present in PSCs associated with gravity waves (Sect. 3.3), could help explain the observed East/West depolarization imbalance. However, the depolarization distribution is not solely influenced by temperature: isolated geographical regions (Sect. 3.2) reveal depolarization distributions clearly centered on high values (e.g. 0.4) that are not associated with cold temperatures. Individual locations present strongly typed depolarization ratios, with average values of 0.4, 0.2 or 0, but at such locations the δ distribution is rarely monomodal, emphasizing the frequent simultaneous occurrence of various microphysics in the same vicinity. The δ distribution is frequently quite large, which is symptomatic of a solid/liquid particle mix; its general shape gives primary importance to zero depolarization, typical of STS. Both observations agree with results of the PSC classification scheme: a majority of mixed clouds and STS, consistent with long-term lidar climatologies of PSCs observed in Arctic by Blum et al. (2005) and Massoli et al. (2006). A visual examination of backscatter images suggests the dominance of mixed clouds is due to the omnipresence of extended stacked clouds of different types rather than in-cloud mixing, but further work is needed to verify this assertion. Moreover, the classification reveals 1) a strong increase in ice PSCs during the end of July, correlated with a comparable decrease in STS PSCs, 2) a higher frequency of STS PSCs at the beginning and the end of the winter season, anticorrelated with frequency of mixed PSCs. This seasonal cycle suggests a possible balance mechanism between mixed, ice and STS PSC populations, from which NAT-based PSCs are excluded. Since the average depolarization is weighted by cloud backscatter (Sect. 3.3), it is possible that weakly backscattering PSCs are not represented well in present results ; future work will have to assess the importance of such PSCs, including those lying under the scattering ratio detection threshold (Sect. 2), and determine if they possess specific characteristics. Though these clouds only have a limited radiative impact and particulate content, they could still play an important role in the PSC lifecycle by e.g. being initiators of cloud formation.

Orography plays a limited but important role, as some PSCs over the Antarctic peninsula and Western coastline (06/16-07/16) appear linked to gravity waves (Small-Scale Variabil-

ity PSCs in Adriani et al. 2004). These clouds reach extremely high altitudes (higher than 26 km) and are optically thicker than other PSCs by an order of magnitude, although geometrically thin. Their depolarization distribution is bimodal centered on 0 and 0.4, similar to the case observed over Scandinavia in Dörnbrak et al. (2002). They represent a minority however when compared to the entire PSC population.

As a final note, this study shows that spatially-resolved results can be obtained through active remote sensing over synoptic-scale areas and extended time periods; this confirms the importance of CALIPSO for the study of optically thin clouds on a global scale.

Acknowledgments: the authors would like to thank J. Pelon, A. Garnier, K. Ramage and S. Bouffies-Cloche for their help with the access to CALIOP data, its storage and analysis. The authors would also like to thank anonymous Reviewers for their useful suggestions.

References

Adriani A., P. Massoli, G. Di Donfrancesco, F. Cairo, M. L. Moriconi and M. Snels, 2004: Climatology of polar stratospheric clouds based on lidar observations from 1993 to 2001 over McMurdo station, Antarctica. *J. Geophys. Res.* **109** D24211.

Beyerle G., M. R. Gross, D. A. Haner, N. T. Kjome, I. S. McDermid, T. J. McGee, J. M. Rosen, H.-J. Schafer and O. Schrems 2001: A Lidar And Backscatter Sonde Measurement Campaign At Table Mountain During February-March 1997: Observations Of Cirrus Clouds. *J. Atmos. Sci.* **58** 1275-1287.

Biele J., A. Tsias, B. P. Luo, K. S. Carslaw, R. Neuber and co-authors 2001: Nonequilibrium coexistence of solid and liquid particles in Arctic stratospheric clouds. *J. Geophys. Res.* **106** 22991-23007.

Blum U., K. H. Fricke, K. P. Müller, J. Siebert and G. Baumgarten, 2005: Long-term lidar observations of polar stratospheric clouds at Esrange in northen Sweden. *Tellus* **57B** 412-422.

Browell E. V., C. F. Butler, S. Ismail, P. A. Robinette, A. F. Carter and co-authors 1990: Airborne lidar observations in the wintertime arctic stratosphere: polar stratospheric clouds. *Geophys. Res. Let.* **17** 385-388.

Browell E. V., S. Ismail and W. B. Grant 1998: Differential absorption lidar (DIAL) measurements from air and space. *Appl. Phys. B* **67** 399-410.

David C., S. Bekki, S. Godin, G. Mégie and M. P. Chipperfield 1998: Polar Stratospheric Clouds climatology over Dumont d'Urville between 1989 and 1993 and the influence of volcanic aerosols on their formation, *J. Geophys. Res.* **103** 22163-22180.

Dörnbrack A., T. Birner, A. Fix, H. Flentje, A. Meister, H. Schmid, E. V. Browell and M. J. Mahoney, 2002: Evidence for inertia gravity waves forming polar stratospheric clouds over Scandinavia. *J. Geophys. Res.* **107** (D20) 8287.

Drdla K. and E. V. Browell, 2004: Microphysical modeling of the 1999-2000 Arctic winter: 3. Impact of the homogeneous freezing on polar stratospheric clouds. *J. Geophys. Res.* **109** D10201.

Eckermann, S. D., Dörnbrack, A., Vosper, S. B., Flentje, H., Mahoney, M. J., Bui, T. P., and Carslaw, K. S.: Mountain wave-induced polar stratospheric cloud forecasts for aircraft science flights during SOLVE/THESEO 2000, Wea. Forecasting **21**, 42– 68, 2006.

Farman J. C., B. G. Gardiner and J. D. Shanklin, 1985: Large Losses of Total Ozone in Antarctica Reveal Seasonal ClOx/NOx Interaction. *Nature* **315**, 207-210.

Fahey D. W. et al., 2001: The Detection of Large HNO_3-Containing Particles in the Winter Arctic Stratosphere. *Science* **291** 1026-1031.

Fromm M., J. Alfred and M. Pitts, 2003: A unified, long-term, high-latitude stratospheric aerosol and cloud database using SAM II, SAGE II, and POAM II/III data: Algorithm description, database definition, and climatology. *J. Geophys. Res.* **108** (D12) 4366.

Fueglistaler, S., B. P. Luo, S. Buss, H. Wernli, C. Voigt, M. Müller, R. Neuber, C. A. Hostetler, L. R. Poole, H. Flentje, D. W. Fahey, M. J. Northway, Th. Peter 2002 : Large NAT particle formation by mother clouds: Analysis of SOLVE/THESEO-2000 observations. *Geophys. Res. Let.* **29** (12) 1610.

Gobiet A., U. Foelsche, A. K. Steiner, M. Borsche, G. Kirchengast, J. Wickert, 2005: Climatological validation of stratospheric temperatures in ECMWF operational analyses with CHAMP radio occultation data. *Geophys. Res. Let.* **32** L12806.

Hertzog A., F. Vial, A. Dörnbrack, S. D. Eckermann, B. M. Knudsen and J.-P. Pommereau, 2002: In-situ observations of gravity waves and comparisons with numerical simulations during the SOLVE/THESEO 2000 campaign. *J. Geophys. Res.* **107** (D20), 8292.

Hervig M. E., K. L. Pagan, P. G. Foschi, 2001: Analysis of polar stratospheric cloud measurements from AVHRR. *J. Geophys. Res.* **106** (D10), 10363-10374.

Höpfner M., N. Larsen, R. Spang, B. P. Luo, J. Ma, S. H. Svendsen, S. D. Eckermann, B. Knudsen, P. Massoli, F. Cairo, T. v. Clarmann and H. Fischer 2006: MIPAS detects Antarctic stratospheric belt of NAT PSCs caused by mountain waves. *Atmos. Chem. Phys.* **6** 1221-1230.

Hostetler, C. A., Liu, Z., Reagan, J., Vaughan, M., Winker, D., Osborn, M., Hunt, W. H., Powell, K. A., Trepte, C. 2006: CALIOP Algorithm Theoretical Basis Document- Par t 1: Calibration and Level 1 Data Products, PC-SCI-201, NASA Langley Research Center, Hampton, VA.
Available at: http://www-calipso.larc.nasa.gov/resources/project/documentation.php

Hudson S. R. and R. E. Brandt, 2005: A look at the Surface-Based Temperature Inversion on the Antarctic Plateau. *J. Clim.* **18** 1673-1696.

Jensen, E. J., O. B. Toon, A. Tabazadeh, and K. Drdla, 2002: Impact of polar stratospheric cloud particle composition, number density, and lifetime on denitrification. J. of Geophys. Res. **107** (D20) 8284.

Lowe D., A. R. MacKenzie, H. Schlager, C. Voigt, A. Dörnbrack, M. J. Mahoney and F. Cairo, 2006: Liquid particle composition and heterogeneous reactions in a mountain wave Polar Stratospheric Cloud. *Atmos. Chem. Phys.* **6** 3611-3623.

Massoli P., M. Maturilli and R. Neuber, 2006: Climatology of Arctic polar stratospheric clouds as measured by lidar in Ny-Alesund, Spitsbergen (79°N, 12°E). *J. Geophy. Res.* **111** D09206.

McGill M., M. A. Vaughan, C. R. Trepte, W. D. Hart, D. L. Hlavka, D. M. Winker and R. E. Khuen 2007: Airborne validation of spatial properties measured by the CALIPSO Lidar. *J. Geophys. Res.* in press.

Nash E. R., P. A. Newman, J. E. Rosenfield and . R. Schoeberl, 1996: An objective determination of the polar vortex using Ertel's potential vorticity. *J. Geophys. Res.* **101** (D5), 9471-9478.

Palm S. P., A. Benedetti, J. Spinhirne, 2005a: Validation of ECMWF global forecast model parameters using GLAS atmospheric channel measurements. *Geophys. Res. Let.* **32** L22S03.

Palm S. P., M. Fromm and J. Spinhirne 2005b: Observations of Antarctic Polar Stratospheric Clouds by the Geoscience Laser Altimeter System. *Geophys. Res. Let.* **32** L22S05.

Pavolonis M. J. and J. R. Key, 2003: Antarctic Cloud Radiative Forcing at the Surface Estimated from the AVHRR Polar Pathfinder and ISCCP D1 Datasets, 1985-93. *J. Appl. Met.* **42** 827-840.

Poole R., S. Solomon, M. P. McCormick and M. C. Pitts, 1989: Interannual variability of PSCs and related parameters in Antarctica during September and October. *Geophys. Res. Let.* **16** (10) 1157-1160.

Poole R. and Pitts, 1994: Polar stratospheric cloud climatology based on SAM II observations from 1978 to 1989. *J. Geophys. Res.* **99** (D6) 13083 - 13089.

Randel W. J. 2001: Middle Atmosphere: Zonal mean climatology. Encyclopedia of Atmospheric Sciences, Academic Press.

Santacesaria V., R. McKenzie and L. Stefanutti 2001: A climatological study of polar stratospheric clouds (1989-1997) from lidar measurements over Dumont d'Urville (Antarctica). *Tellus* **53** 306-321.

Sassen K., 1991: The polarization lidar technique for cloud research : a review and current assessment. Bull. of Am. Meteor. Soc. **71** 1848-1866.

Sassen K., and S. Benson, 2001: A midlatitude Cirrus Cloud Climatology from the Facility for Atmospheric Remote Sensing. Part II : microphysical properties derived from lidar depolarisation. *J. of Atmos. Sci.* **58** 2103-2111.

Savigny C. von, E. P. Ulasi, K.-U. Eichmann, H. Bovensmann and J. P. Burrows 2005: Detection and mapping of polar stratospheric clouds using limb scattering observations. *Atmos. Chem. Phys.* **5** 3071-3079.

Solomon S. 1999: Stratospheric ozone depletion: A review of concepts and history. *Reviews of Geophysics* **37** 275-316.

Spang R., M. Riese and D. Offermann, 2001: CRISTA-2 observations of the south polar vortex in winter 1997: A new dataset for polar process studies. *Geophys. Res. Let.* **28** 3159-3162.

Spang R., J. J. Remedios, L. J. Kramer, L. R. Poole, M. D. Fromm, M. Müller, G. Baumgarten and P. Konopka, 2005: Polar stratospheric cloud observations by MIPAS on ENVISAT: detection method, validation and analysis of the northern hemisphere winter 2002/2003. *Atmos. Chem. Phys.* **5**, 679-692.

Spihirne J. D., S. P. Palm, W. D. Hart, D. L. Hlavka, E. J. Welton, 2005a: Cloud and aerosol measurements from GLAS: Overview and initial results. *Geophys. Res. Let.* **32** L22S03.

Spinhirne J. D., S. P. Palm and W. D. Hart, 2005b: Antarctica cloud cover for October 2003 from GLAS satellite lidar profiling. *Geophys. Res. Let.* **32** L22S05.

Stefanutti L., M. Morandi, M. del Guasta, S. Godin and C. David 1995: Unusual PSC observed by lidar in Antarctica. *Geophys. Res. Let.* **22** 2377-2380.

Stein B., C. Wedekind, H. Wille, F. Immler, M. Müller, L. Wöste, M. del Guasta, M. Morandi, L. Stefanutti, A. Antonelli, P. Agostini, V. Rizi, G. Readelli, V. Mitev, R. Matthey, R. Kivi and E. Kyrö, 1999: Optical classification, existence temperatures, and coexistence of different polar stratospheric cloud types. *J. Geophys. Res.* **104** (D19) 23983-23993.

Teitelbaum, H., M. Moustaoui, and M. Fromm, 2001: Exploring Polar Stratospheric Cloud and Ozone Minihole Formation: The primary Importance of Synoptic-Scale Flow Perturbations. *J. of Geophys. Res.* **106** (D22) 28173-28188.

Toon O. B., E. V. Browell, S. Kinne and J. Jordan, 1990: An analysis of lidar observations of polar stratospheric clouds. *Geophys. Res. Let.* **17** 393-396.

Toon O. B., A. Tabazadeh, E. V. Browell and J. Jordan 2000: Analysis of lidar observations of Arctic polar stratospheric clouds during January 1989. *J. Geophys. Res.* **105** 20589-20615.

Tsias A., M. Wirth, K. S. Carslaw, J. Biele, H. Mehrtens and co-authors 1999: Aircraft lidar observations of enhanced type Ia PSCs during APE-POLECAT. *J. Geophys. Res.* **104** 23961-23969.

Wang X. and D. V. Michelangeli, 2006: Comparison of microphysical modeling of polar stratospheric clouds against balloon-borne and Improved Limb Atmospheric Spectrometer (ILAS) satellite observations. *J. Geophys. Res.* **111** D10201.

Winker D. M., J. Pelon, M. P. McCormick 2003: The CALIPSO mission: Spaceborne lidar for Observation of Aerosols and Clouds. *Proc. SPIE* **4893**, pp. 1-11.

Winker D. M., W. H. Hunt and C. A. Hostetler, 2004: Status and Performance of the CALIOP lidar. *Proc. SPIE* **5575**, pp. 8-15.

Winker D. M., M. Vaughan, B. Hunt 2006: The CALIPSO mission and initial results from CALIOP. *Proc. SPIE* **6409**, 640902.

Winker D. M., B. Hunt and M. McGill 2007: Initial Performance Assessment of CALIOP. *Geophys. Res. Let.* in press.

WMO: Scientific Assessment of Ozone Depletion: 2002, Report 47, Global Ozone Research and Monitoring Project, Geneva, 2003.

You Y., G. W. Kattawar, P. Yang, Y. Hu, and B. A. Baum 2006: Sensitivity of depolarized signals to cloud and aerosol particle properties. *J. Quant. Spectrosc. Radiat. Transfer* **100** 470-482.

Figure Captions

Fig. 1: a) Example of attenuated backscatter from a PSC observed from CALIPSO on July 24th 2006. Color scale is logarithmic. Average backscatter profile is shown in the right pane. b) Result of the cloud detection, with clear sky showing up as white.

Fig. 2A. Columns, from left to right: Geographic distribution for the first 5 weeks (June 16-July 24) of the a) percentage of profiles with at least three cloudy points above 13 km, b) cloud thickness above 13 km, c) minimum temperature on the 530 K isentropic surface and d) depolarization ratio in cloudy points, weekly averaged in 2.5°×2.5° boxes. For the first week (June 16 to June 23), some cells are not filled due to the missing lidar profiles. The black line shows the polar vortex (Nash et al. 1996), averaged on a 36h period centered in the middle of each week. The Antarctica coastline is superimposed. Fig. 2B : same as Fig. 2A, for the five last weeks of the considered period (July 24-August 31).

Fig. 3: Temperature distribution in all stratospheric cloudy points between June 14 and August 31st.

Fig. 4: Distributions of altitudes and depolarization in cloudy points, at temperatures warmer and colder than 188K.

Fig. 5: Distribution of PSCs as a function of scattering ratio and depolarization ratio, using a logarithmic color scale. Areas are identified using boundaries from Table 1 in Massoli et al. 2006.

Fig. 6: Percentages of PSC types as a function of time using the Massoli et al. classification scheme.

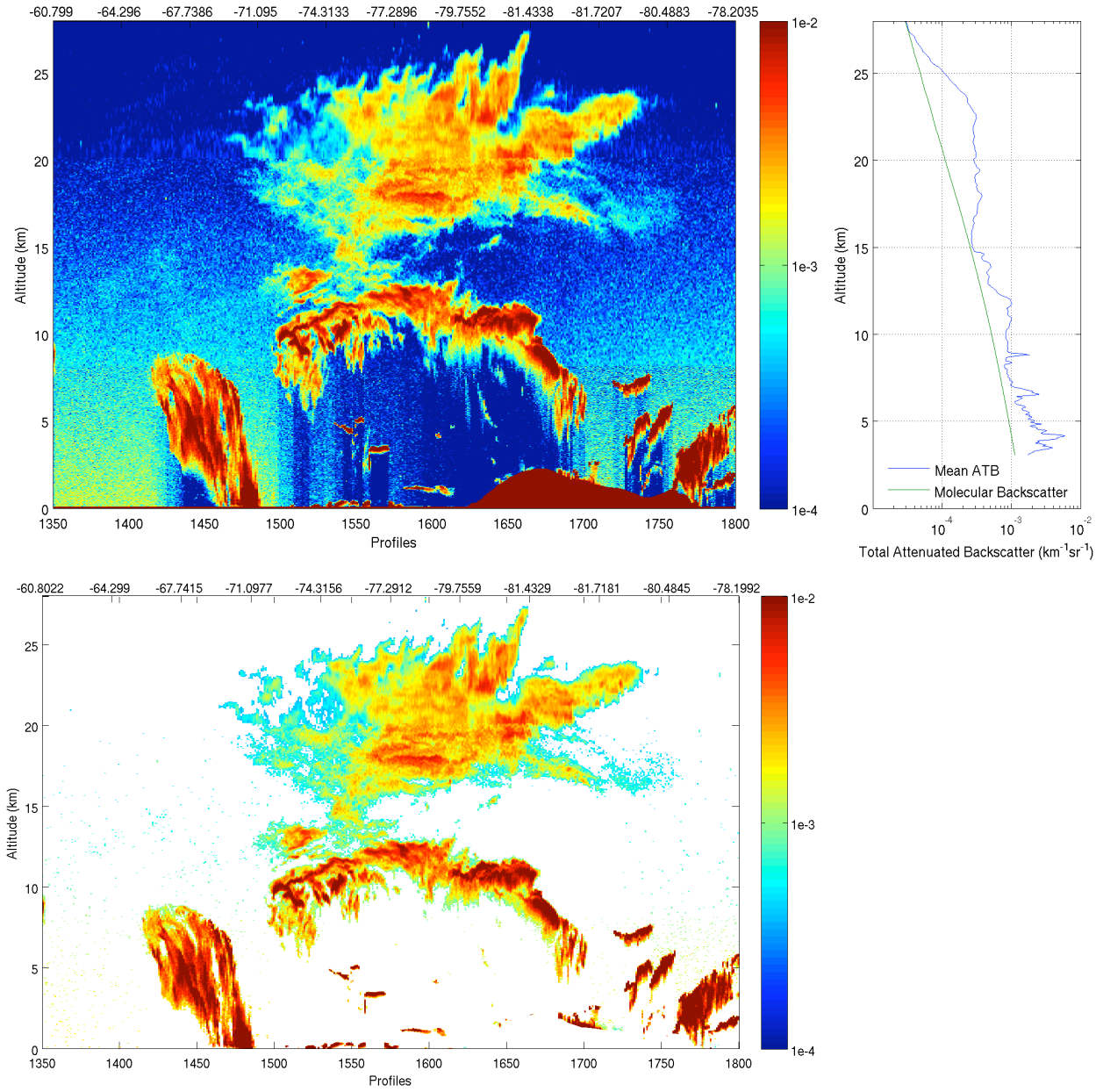

Fig. 1: a. Example of attenuated backscatter from a PSC observed from CALIPSO on July 24th 2006. Color scale is logarithmic. Average backscatter profile is shown in the right pane. b. Result of the cloud detection, with clear sky in white.

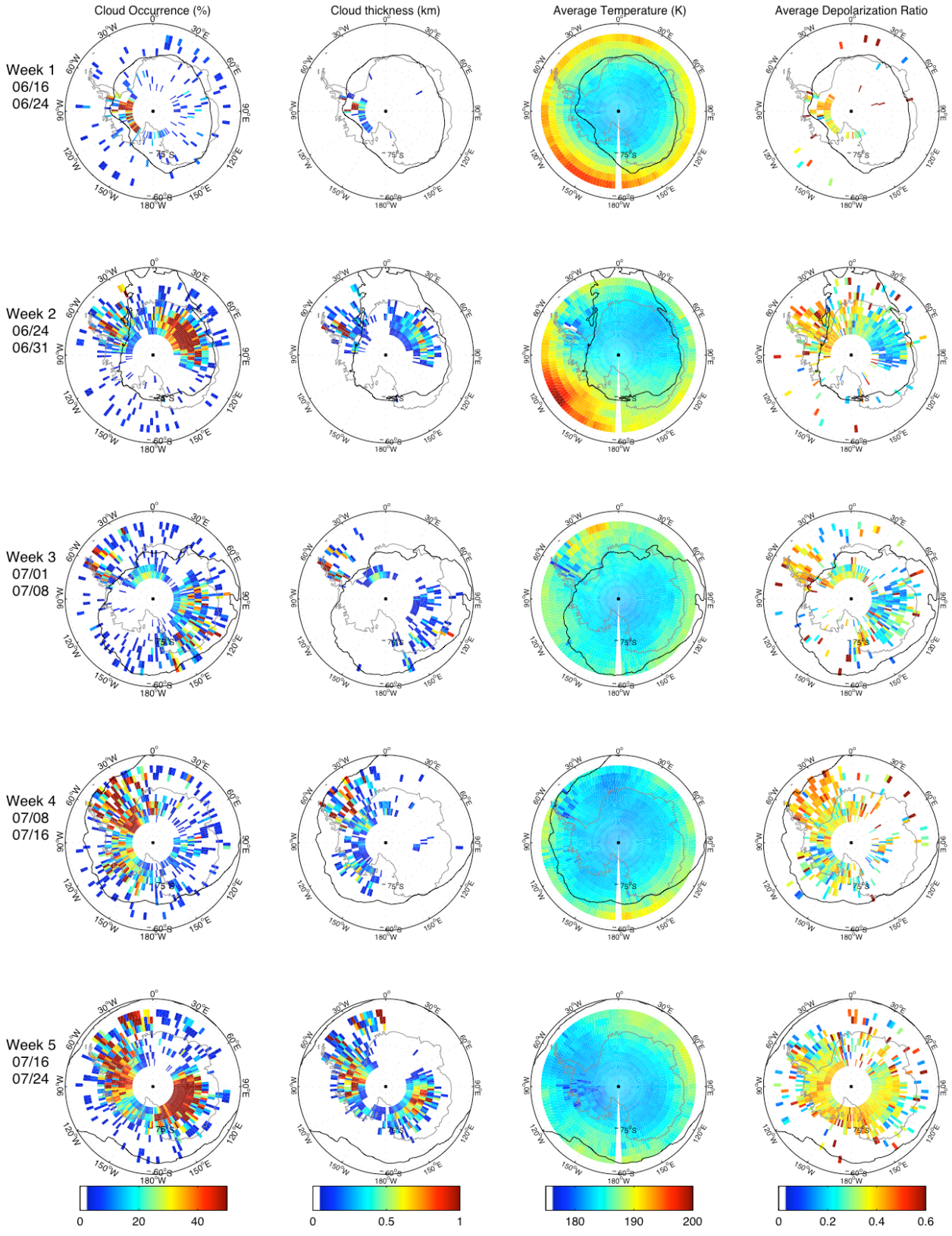

Fig. 2A. Columns, from left to right: Geographic distribution for the first 5 weeks (June 16-July 24) of the a) percentage of profiles with at least three cloudy points above 13 km, b) cloud thickness above 13 km, c) minimum temperature on the 530 K isentropic surface and d) depolarization ratio in cloudy points, weekly averaged in 2.5°×2.5° boxes. For the first week (June 16 to June 23), some cells are not filled due to the missing lidar profiles. The black line shows the polar vortex (Nash et al. 1996), averaged on a 36h period centered in the middle of each week. The Antarctica coastline is superimposed in grey.

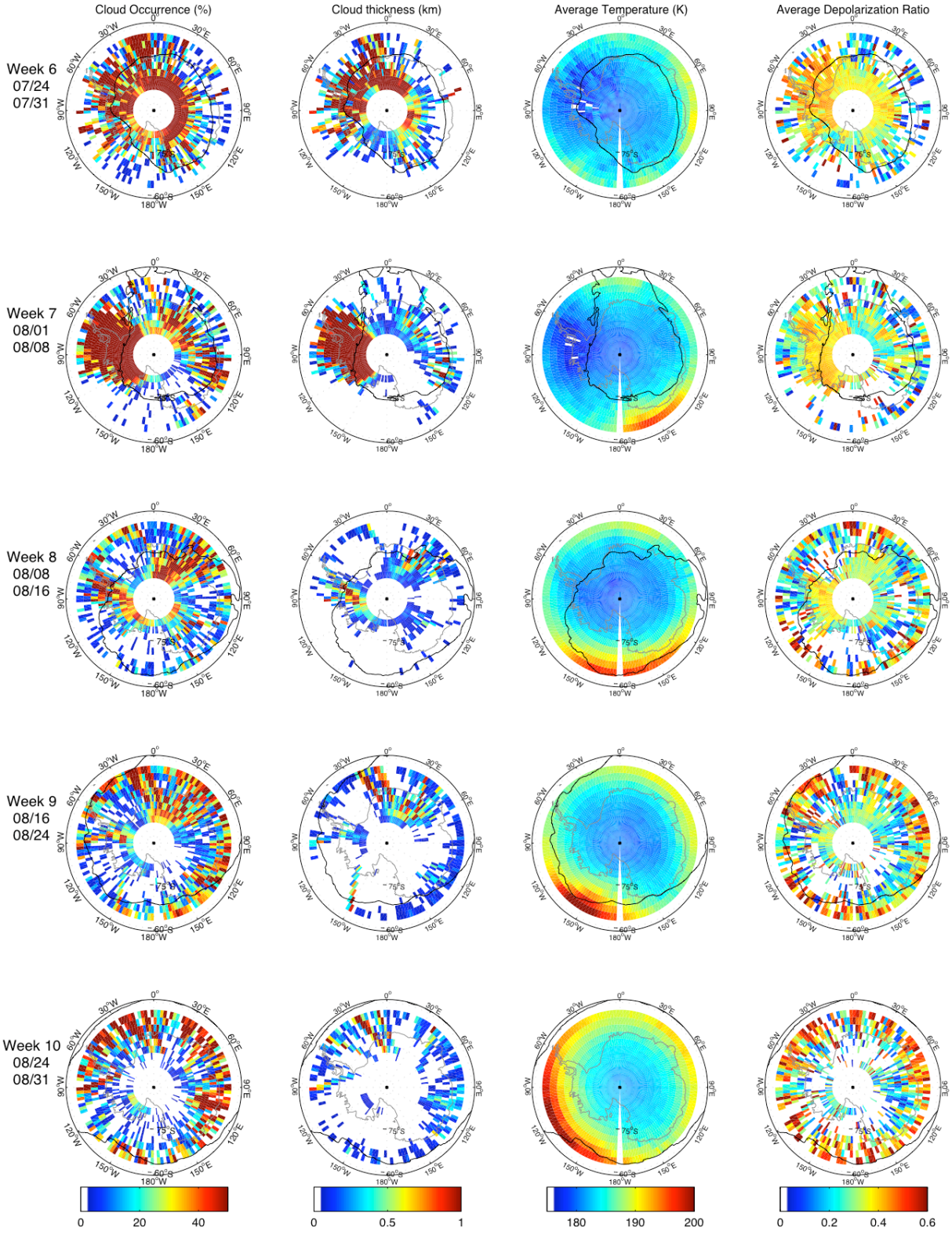

Fig. 2B : same as Fig. 2A, for the five last weeks of the considered period (July 24-August 31).

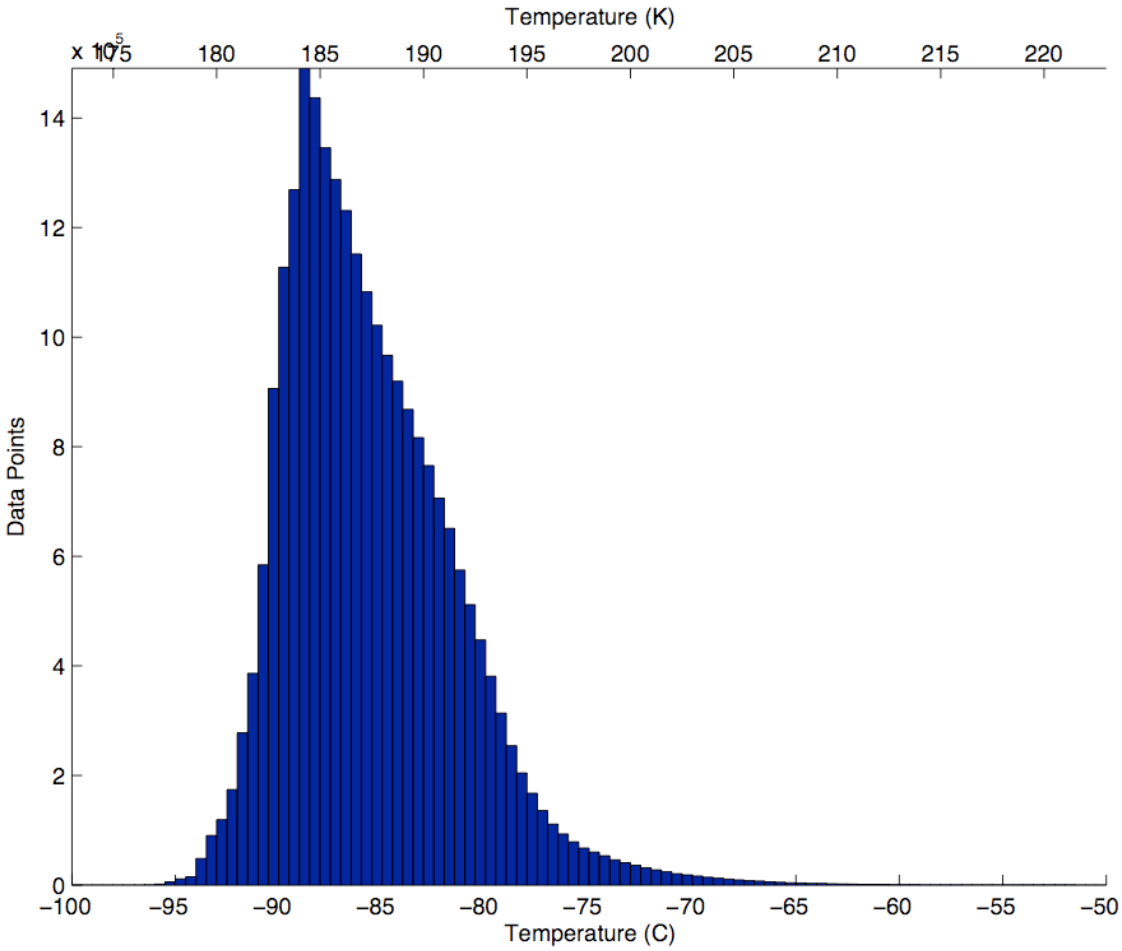

Fig. 3: Temperature distribution in stratospheric cloud points between June 14 and August 31st.

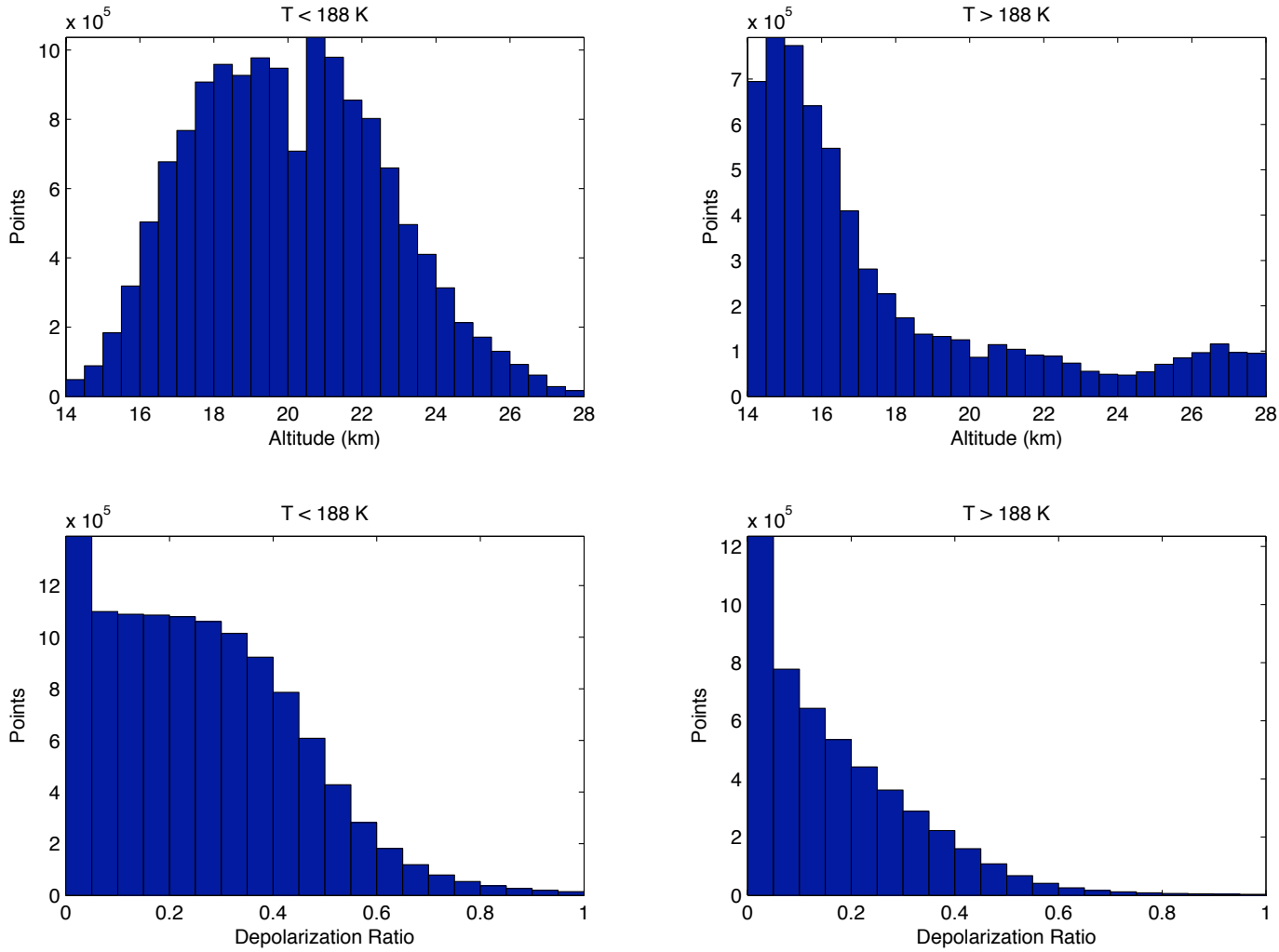

Fig. 4: Distributions of altitude and depolarization for cloud points at temperatures colder and warmer than 188K.

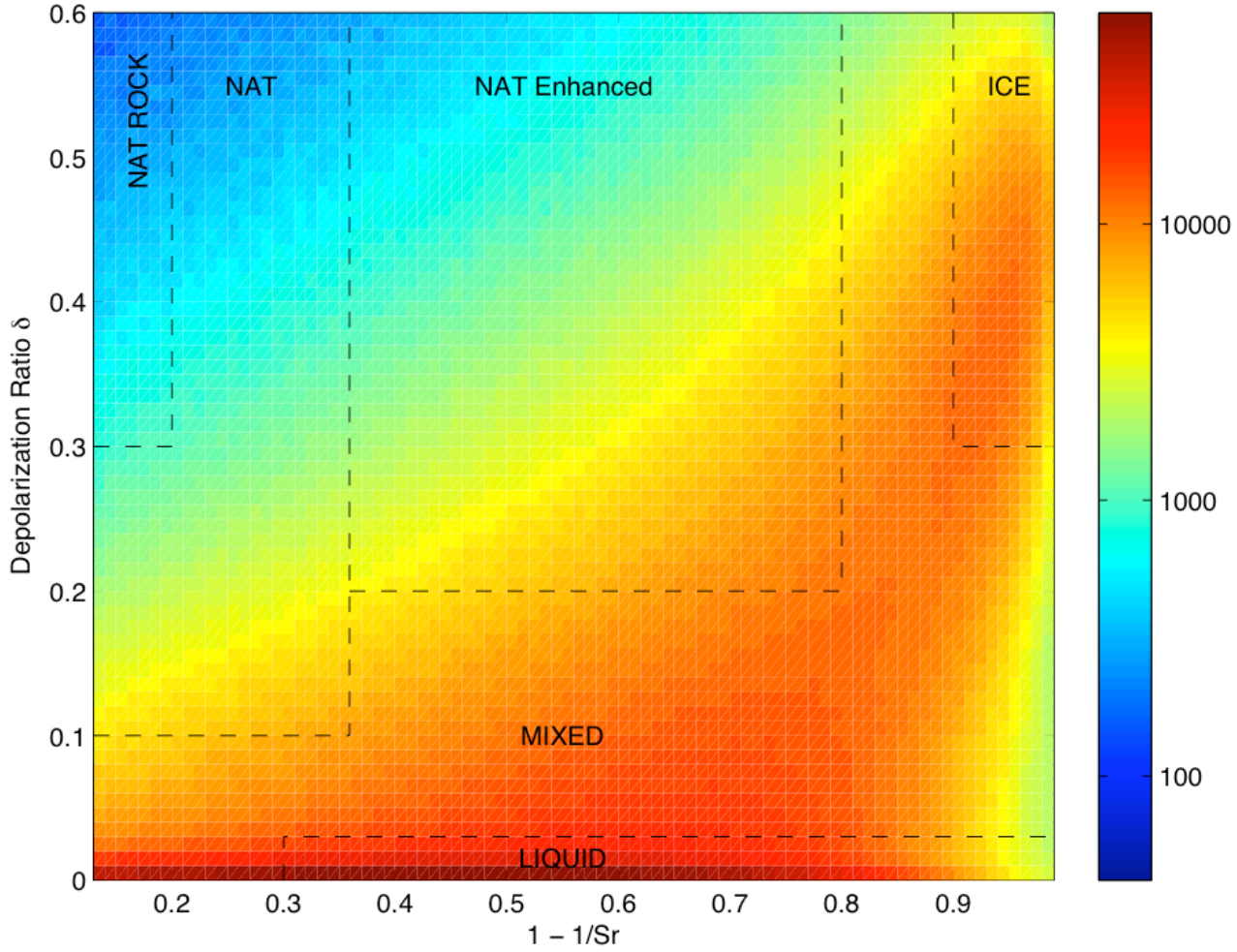

Fig. 5 : 2D distribution of PSCs (in number of points) as a function of scattering ratio and depolarization ratio, using a logarithmic color scale. Areas are identified using boundaries from Table 1 in Massoli et al. 2006.

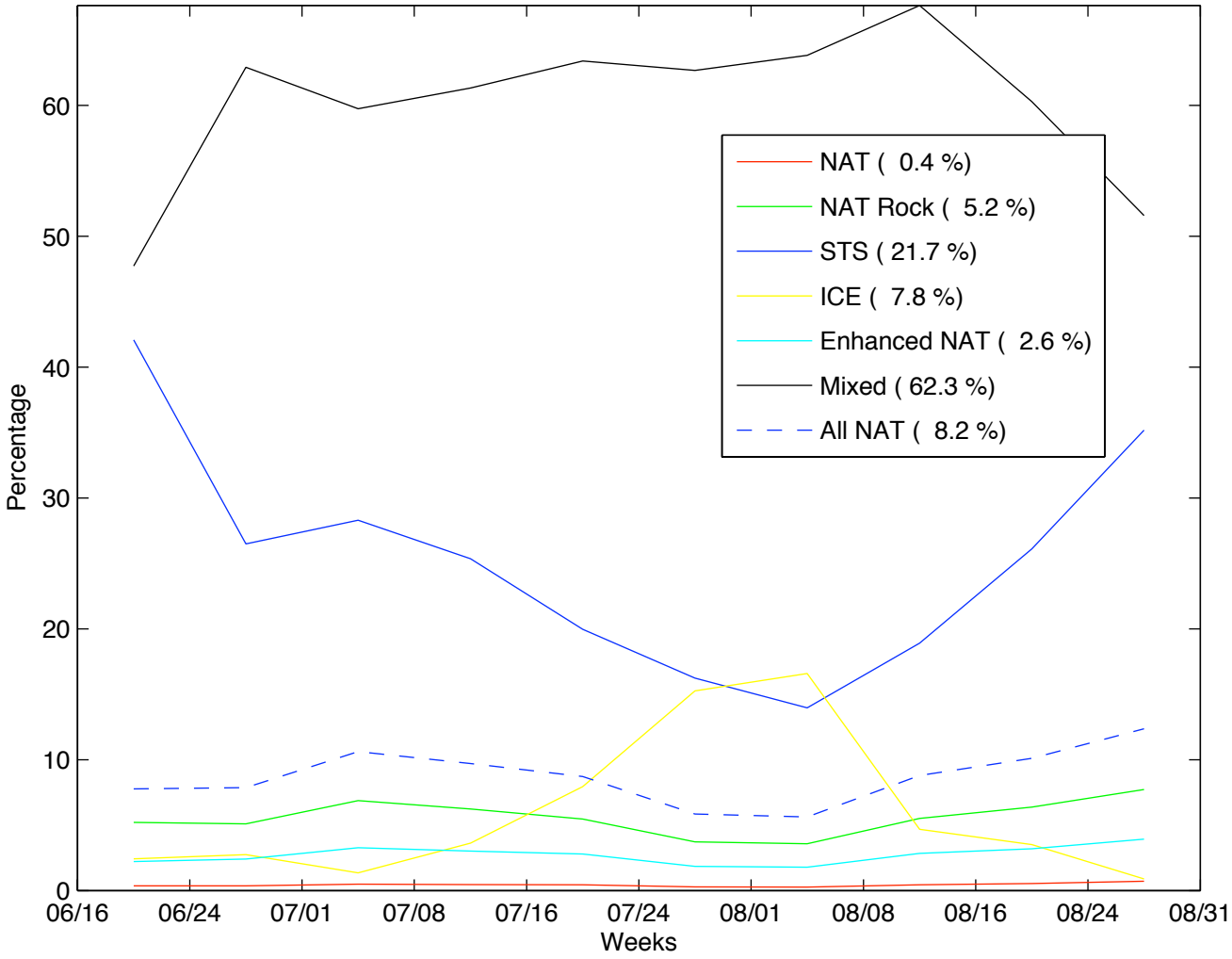

Fig. 6: Percentages of PSC types as a function of time using the Massoli et al. classification scheme.